A Multiresolution Image Segmentation Technique Based on Pyramidal Segmentation and Fuzzy Clustering

Mahmoud Ramze Rezaee, Pieter M. J. van der Zwet, Boudewijn P. F. Lelieveldt, Rob J. van der Geest, and Johan H. C. Reiber, *Senior Member, IEEE*

***Abstract*—In this paper, an unsupervised image segmentation technique is presented, which combines pyramidal image segmentation with the fuzzy c-means clustering algorithm. Each layer of the pyramid is split into a number of regions by a root labeling technique, and then fuzzy c-means is used to merge the regions of the layer with the highest image resolution. A cluster validity functional is used to find the optimal number of objects automatically. Segmentation of a number of synthetic as well as clinical images is illustrated and two fully automatic segmentation approaches are evaluated, which determine the left ventricular volume (LV) in 140 cardiovascular magnetic resonance (MR) images. First fuzzy c-means is applied without pyramids. In the second approach the regions generated by pyramidal segmentation are merged by fuzzy c-means. The correlation coefficients of manually and automatically defined LV lumen of all 140 and 20 end-diastolic images were equal to 0.86 and 0.79, respectively, when images were segmented with fuzzy c-means alone. These coefficients increased to 0.90 and 0.94 when the pyramidal segmentation was combined with fuzzy c-means. This method can be applied to any dimensional representation and at any resolution level of an image series. The evaluation study shows good performance in detecting LV lumen in MR images.**

***Index Terms*—Cardiovascular MRI, fuzzy clustering, image pyramids, segmentation.**

I. Introduction

VARIOUS medical imaging modalities such as X-ray, positron emission tomography (PET), computer tomography (CT), and magnetic resonance imaging (MRI) are widely available and used in routine clinical practice. It has been generally accepted that visual interpretation of such images is highly subjective. Quantification by manual tracing of outlines of structures to be studied is tedious, time-consuming and also hampered by significant inter- and intra-observer variabilities. Imaging modalities, which produce multidimensional data sets such as CT and MRI, require the interpretation of tens to hundreds of slices. As a result, there is a great need for automated segmentation techniques that are robust and are characterized by a high degree of accuracy and precision.

Manuscript received December 31, 1997; revised December 13, 1999. This work was supported by the Science Foundation, The Netherlands, under Project LGN22.2781. The associate editor coordinating the review of this manuscript and approving it for publication was Prof. Jeffrey J. Rodriguez.

The authors are with the Division of Image Processing, Department of Radiology, Leiden University Medical Center, 2300 RC Leiden, The Netherlands (e-mail: hreiber@lkeb.azl.nl).

Publisher Item Identifier S 1057-7149(00)05322-7.

Application of various automatic and semi-automatic segmentation methods in cardiac imaging has grown in recent years [1]–[13]. Segmentation methods for a number of applications [4]–[7] are based on deformable contour models such as snakes, which conform to various heart shapes and motions. By this approach an initial snake (mostly outlined manually around an anatomical object of interest) is deformed under the internal (bending) and external forces (lines, edges, features of an image, etc.), converging to a final form corresponding with an equilibrium energy state. In addition, in [9] Goshtasby used a generalized cylinder as an elastic curve to represent the ventricular boundaries.

Minimum cost edge detection has been applied in [1], [8], and [12] to find the left ventricular boundaries. Active shape models have also been applied in [11] to define the left ventricle in both long axis and short axis echocardiograms. By this approach an initial average model of the left ventricle and its associated structures undergo shape deformations that are consistent with a statistical model derived from a number of echocardiographic images. By considering segmentation as a pixel classification task, the fuzzy c-means algorithm has also been applied in [2], [10] and [13] to define the left ventricular boundary in MR images.

Usually, segmentation of medical images is based on information from a single image. Due to various noise contributions the information within a single image is not sufficient to obtain a reliable segmentation. Therefore, in general, segmentation methods that operate on multiple images, either connected in space or time, will improve the final segmentation of each image.

In the following, we will describe a general unsupervised segmentation technique. This segmentation method is based on the combination of pyramidal segmentation and fuzzy clustering. Our method can be applied to a series of images that are represented by two-dimensional (2-D), three-dimensional (3-D) or N-dimensional (ND) representations. In Section II the background of the method is presented, including the pyramidal representation and segmentation technique and the fuzzy c-means clustering algorithm. Section III describes the image data that is used in the evaluation study. In Section IV, the segmentation results of some synthetic as well as clinical examples of different imaging modalities are presented. This section also includes the results of a validation study, which evaluates the automatically and manually defined segmentation results of 140 MR images of infarct abnormal subjects having a clinical his-

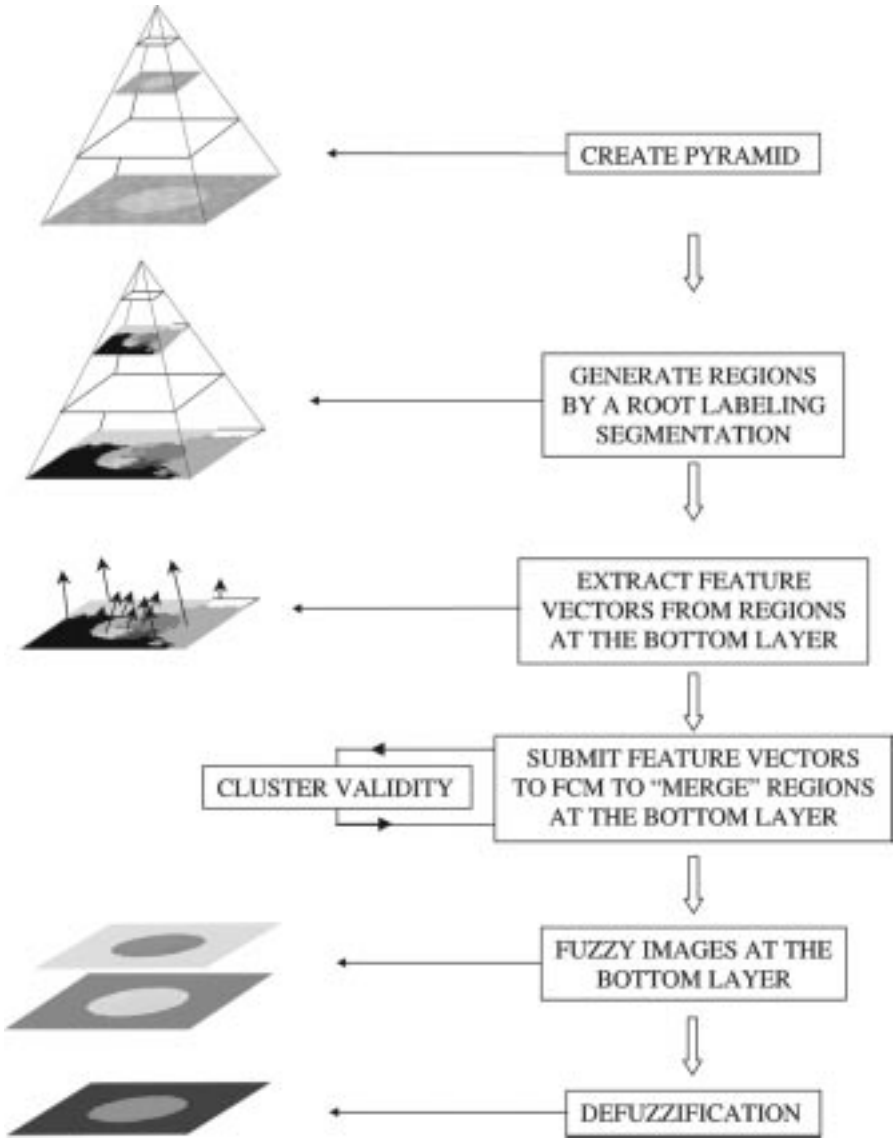

Fig. 1. General format of our automatic segmentation procedure.

tory of cardiac disease, and normal volunteers without a known history of heart disease. Furthermore, the segmentation results obtained by applying only fuzzy clustering, and also the results of pyramidal segmentation in combination with fuzzy clustering are presented in Section IV. In Section V, the results are summarized and discussed.

II. Method

A general outline of our automatic segmentation procedure is presented in Fig. 1. The operator should only select an image (or an image series) and a range of possible object numbers. Each layer of the pyramid may contain one image, as it is shown in the Fig. 1, or an image series. The images at different layers represent various image resolutions. Images are first split into a number of regions by the pyramidal segmentation. Fuzzy c-means is then applied to merge all regions at the bottom layer of the pyramid into a number of fuzzy objects. When the number of objects is not known *a priori*, a validity functional can be used to automatically find the number of (fuzzy) objects. Finally, a defuzzification method is applied to each fuzzy image to obtain the final segmentation result.

The following sections provide a summarized theoretical background of the segmentation procedure. The pyramidal representation and segmentation will be described first, followed by the fuzzy c-means algorithm. The reliability of a number of cluster validation indices that allow the assessment of the number of objects in an image is also studied.

A. Pyramidal Approach

1) Pyramidal Representation: Multiresolution methods attempt to obtain a global view of an image by examining it at various resolution levels. Kelly [14] initially suggested a strategy, called planing, based on a first analysis of an image at a reduced resolution, followed by a second, more detailed analysis at a higher resolution. The pyramid data structure has been examined by a number of investigators; see Trivedi and Bezdek [15]. As Fig. 2 shows, by successively reducing the image size using a

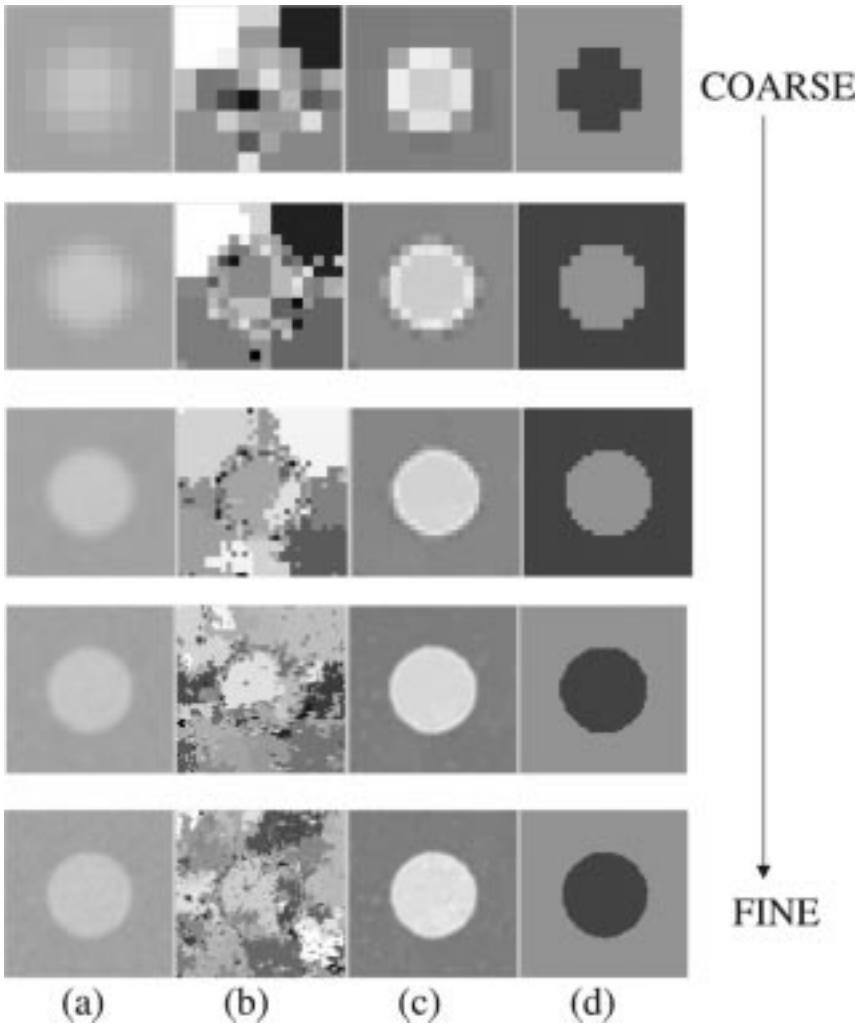

Fig. 2. (a) Gaussian pyramid representation of a synthetic image with $\mathrm{SNR} = 10$ dB, from layer 3 (top image of $8 * 8$ size) to the bottom layer (bottom image of $256 * 256$ size). Note that for display purposes the images of the upper layers were enlarged. (b) Pyramidal segmentation of the image of Fig. 2(a) from layer 4 into the bottom layer. Different gray values of the image elements correspond to different labels. (c) The fuzzy image of the class disk from layer 4 to the bottom layer. The fuzzy image of the class background is not displayed. (d) Defuzzification of the fuzzy images of (c). Each pixel of a layer in an image is assigned to one class.

combination of convolution and sub-sampling a pyramid representation of an image can be obtained. For an image of original size $2^K \times 2^K$, the pyramid representation of an image at the $(n-1)$th layer of the pyramid can be described as

$$f^{n-1}(x,y) = \sum_{i=-N+1}^{N} \sum_{j=-M+1}^{M} C_{ij} * f^n(2x+i, 2y+j) \quad (1)$$

where $f^n(x,y)$ is the gray value of an image at the (x,y) position in the nth layer of the pyramid, C_{ij} is a filter coefficient, $2N$ and $2M$ are the filter sizes. In a Gaussian (low-pass) pyramid [16], the pyramid is constructed by repeated application of local averaging and sub-sampling; see Fig. 2(a). The pyramid can also be built by the difference of low-pass [17] or Laplacian operator, by which specific structures in an image such as blobs (maxima) and ridges can be detected. The pyramid may contain an image series in each layer rather than a single image. For example, a coarse representation of an X-ray or MR image series, acquired over a cardiac cycle, can be represented at different layers of the pyramid, each of which containing all images of the series.

2) Pyramidal Segmentation: Like other segmentation techniques, the primary goal of pyramidal segmentation is to find the location and extent of all objects that exist in an image. A number of pyramidal segmentation techniques exist. Generally, the blurred images represented in each layer of the pyramid are used for segmentation. Segmentation is applied in two stages. Firstly, a parent-child spatial relationship between the image elements of two adjacent layers is defined. Secondly, this relationship is evaluated by means of a similarity measure. Since different segmentation results can be obtained by different definitions of the spatial relationship and the similarity measure, these two concepts are described in more detail in the following:

Spatial relationship between the image elements of two successive layers of the pyramid describes the family relationship between these elements. For example: in a quadtree representation each image element in the layer $n-1$ is the parent of the four nearest image elements (children) in layer n, so that each child has only one parent and therefore no ambiguity exists within the parent-child relationship. In a linked pyramid this relationship is ambiguous. The children of a layer can belong to different parents in the upper layer.

Similarity between a child image element and its possible parents describes how similar they are. By using features of image

elements similarity can be defined, for example by comparing the contrast or texture properties of a child and its possible parent(s). Since feature vectors in a feature space can represent the properties of a child and its potential parents, similarity can be related to the distance (using a specific metric) between the features of a child and its parent.

We used a root labeling technique, which attaches labels to image elements of each layer. This is performed by evaluating the child-parent relationship in each layer of the pyramid. Starting from the top of the pyramid a label is attached to its top image element. Furthermore, the child-parent relationship was validated by a similarity measure that takes the gray-value statistics of potential parents and a child into account. Among the potential parents, the label of a parent with the highest similarity is assigned to the child. Next, a new label is assigned to a child that is too dissimilar to any parent. The validation approach is extended into the next lower layer of the pyramid, and finally, results in the generation of labeled regions in the bottom layer.

The similarity between a child in layer n and a potential parent in layer $n-1$ is defined as

$$\mathrm{Sim}(X_n) = \frac{\sigma_{n-1}^2 - (g(X_n) - \mu_{n-1})^2}{k} \tag{2}$$

where $g(X_n)$ is the gray value of child X in layer n. The average and standard deviation of the gray values of a region that a potential parent belongs to are μ_{n-1} and σ_{n-1}, respectively. The number of image elements of that region is denoted as k. A child inherits the label of the parent having maximum value of similarity. If, during the labeling (segmentation) procedure, some children are too dissimilar to all the parents, a new label is attached to them. The dissimilarity is measured according to

$$|g(X_n) - \mu_{n-1}| + \sigma_{n-1} > T_{n-1} \tag{3}$$

where T_{n-1} is a predefined threshold value for layer $n-1$. In our implementation the difference between the maximum and the minimum value of pixels of the original images was taken into account. If we denote this difference as diff, then for the bottom layer of the pyramid the threshold was defined as

$$T_{\mathrm{bottom}} = \mathrm{diff} * \alpha; \quad \alpha \in (0,1] \tag{4}$$

where α is the split threshold factor. The threshold in upper layers was decreased by a constant factor $\beta (T_{n-1} = T_n/\beta)$. A higher value of β results in a smaller value of the threshold in the upper layers, which in turn will result in the generation of more regions in the upper layers. Therefore the number of regions generated at the bottom layer will increase by setting a higher value for β.

As Fig. 2(b) shows, the number of regions in the labeled images increases during the segmentation process through the layers of the pyramid. Generally, the number of regions generated on the bottom layer of the pyramid is not equal to the true number of objects which really exist in an image; the image is over- or under-segmented. Usually, an object is split up into a number of smaller regions with different labels. The number of these regions depends on the image type, the split threshold factor α and the decreasing threshold factor β. To merge the regions and to obtain a predefined number of objects, we have used the fuzzy c-means clustering algorithm which will be described in the following section.

B. Fuzzy C-Means Clustering

Fuzzy c-means (FCM), an unsupervised clustering algorithm, has been applied successfully to a number of problems involving feature analysis, clustering and classifier design in fields such as agricultural engineering, astronomy, chemistry, geology, image analysis, medical diagnosis, shape analysis, target recognition [18] and image segmentation [2], [10], [13], [15], [19]–[23]. Although the original algorithm dates back to 1973 [24], [25], derivatives have been described with modified definitions for the norm and prototypes for the cluster centers [26]–[28].

Unlabeled data are labeled by minimizing the following generalized within group sum of squared error objective function

$$J_m(U,V;X) = \sum_{k=1}^{n}\sum_{i=1}^{c} u_{ik}^m * (||x_k - v_i||_A)^2 \tag{5}$$

where the membership value $u_{ik} : X \to [0,1]$ defines the grade of membership of a data point x_k to the i-th cluster center, v_i. The number m is a parameter ranging from 1 to ∞, which controls the fuzziness of the resulting partition and the matrix A defines the norm (for $A = I$ the Euclidean distance will be obtained). By initializing the matrix U randomly and computing the cluster prototypes and the membership values after each iteration repeatedly, FCM will converge to a local minimum or a saddle point of J_m. Convergence can be examined by comparing the changes in the cluster centers or the membership values at two successive iteration steps. Finally, to assign each data point to a specific cluster, defuzzification must be applied, e.g., by attaching a data point to a cluster for which the value of the membership is maximal.

FCM defines for each data point an algorithmic label; it is an unsupervised algorithm. To find for each data point its corresponding physical label, a supervising process is needed.

C. Pyramidal Segmentation and Fuzzy Clustering

In an image processing system an image or its derivatives can be represented in various feature spaces. Classification of objects (anatomical tissues) can be achieved by grouping data points in the feature space with the same similarity into clusters. The dimension of the feature space depends on the representation of the image information. An image can be represented in terms of pixels, which are associated with a location and a gray value. It can also be represented by its derivatives, e.g., regions with features like average gray value, standard deviation, gradient or texture value, etc. Features for clustering can be extracted from regions generated by the pyramidal segmentation procedure. Special care has to be taken to use those features which are most representative for the properties of the desired objects. By applying FCM, a partition of the feature vectors into c new regions can be found. In each layer of the pyramid, this provides a coarse representation of the objects. Since the smallest region is set by the pyramidal segmentation, the final resolution of the detected objects is determined by the parameters of the root labeling technique.

Combination of pyramidal segmentation and fuzzy clustering has some advantages for both techniques. As mentioned above,

the number of regions generated by the pyramidal segmentation procedure is usually larger than the real number of objects in the image. By fixing the number of clusters (objects) *a priori*, FCM essentially merges many small regions into c larger ones, so a predefined number of objects will be found. Since the computational complexity of FCM depends on, among other parameters, the number of patterns and features being clustered, pyramidal segmentation can reduce these numbers drastically by generating a region vector instead of using each image element thereby reducing the computational overhead of FCM. In addition, the pyramidal approach may eliminate local minima of J_m [(5)] that otherwise might trap FCM. Another interesting result of the combination of the pyramidal segmentation and FCM is that the finally defined objects are not crisp but fuzzy. This means that for each image element the membership values of objects are defined. By using these membership values c *fuzzy images* of the fuzzy objects can be constructed. A fuzzy image of a fuzzy object is an image representation of that object. Such an image is shown in Fig. 2(c), where the gray value of each image element is proportional to the membership value. Image elements with a higher membership value are brighter (higher gray value) than those with a lower membership value. Since these images are not crisp (binary) but fuzzy, they can be used as the inputs of a reasoning system. Also, various defuzzification strategies can be applied to obtain the final segmentation. For example, assigning an image element to an object using its maximum membership value [Fig. 2(d)] is called the MAX defuzzification method. Although this defuzzification approach is used in our evaluation study, other defuzzification strategies might be reliable for different applications. For example, a defuzzification strategy can take the membership values of only one fuzzy object into account. In this case all image elements of each fuzzy object which have a membership value greater than a threshold value (called α-cuts) are assigned to the fuzzy object.

D. Cluster Validity Index

For a fully automated segmentation method it is desirable to determine the number of objects within an image automatically. Since regions within a volume of interest (VOI) (generated by the pyramidal segmentation) are represented as groups of clusters in the cluster space, the number of objects within a VOI can be determined automatically by the identification of the number of clusters in the cluster space. Cluster validation indices can be used for this purpose.

We have examined the reliability of five validation indices shown in Table I for determination of the number of objects within the VOI of MR images studied below.

By applying FCM, varying the fuzzy index $m \in (1, \infty)$, and also using different values of $c \in \{c_{\min}, \ldots, c_{\max}\}$, an optimal number of clusters is found for each validation index.

E. Segmentation Procedure Applied to MRI

The two step segmentation procedure described in previous paragraphs was applied to MR images in our validation study. The Hough transform [34] was applied to all images of the same series to obtain a rough estimate of the center of the LV lumen. Around this center point in each image of the image series, a 64×64 region of interest (ROI) image was defined. This results in a 3D volume of interest (VOI), which includes the left- as well as the right ventricular lumen (class blood), papillary muscles (class muscles), lung and background (class background). Only voxels within this VOI are considered for segmentation. To compare the segmentation results of two different methods a VOI is segmented twice. In the first method, FCM is applied directly to the gray values of voxels within a VOI. In the second approach, 3-D regions (within a VOI) generated at the bottom layer of the pyramid are merged by processing feature vectors extracted from them (one per region) with FCM to obtain a more refined (coarser) estimate of objects in the bottom layer. The features used by FCM were the mean and the standard deviation of gray values of voxels of each region. In both approaches FCM produces fuzzy images. The number of images is equal to the number of images in the series multiplied by c, the number of objects looked for.

The LV lumen in the fuzzy images was found in two stages. First the images of the fuzzy class blood were found by using the knowledge that blood has a high gray value in those images. This results in finding the images belonging to the blood class. In the second step the right ventricle lumen is excluded from the LV lumen. This is performed by applying a 3D seeded volume growing technique [35], which uses the center of the LV lumen position, obtained by the Hough transform, as an initial seed point in the first fuzzy image of class blood and propagates this point through all fuzzy images of that class.

F. Evaluation Approach

1) Segmentation Evaluation: To evaluate both automatic segmentation methods, the contour of the LV lumen (excluding papillary muscles) in each image of the MRI validation study was manually delineated by an expert. The manually and automatically defined LV lumens were compared quantitatively by two regression analyses. For each segmentation method described above, two regression studies were carried out on the amount of blood within the LV lumen defined automatically and manually. The first analysis includes the results of all 140 MR images, the second one includes only the results of 20 end-diastolic images. The amount of blood was estimated by multiplying the area of LV lumen with a constant value taking into account the field of view, the image sizes and slice thickness and the gap between slices. This constant factor was for normal and abnormal groups equal to 0.0244, 0.0269, respectively.

2) Validity Indices Evaluation: Different validity indices were applied to fuzzy partitions of the data of the MRI evaluation study. FCM was applied to data that was obtained from the features of regions in the bottom layer of the pyramid. This layer included the VOI of image series of each subject. By means of the gray value of voxels in a VOI three classes could be recognized; the class of blood (within the left as well as the right ventricle) having a high gray value, the class of muscle (the papillary muscle and the myocardium) with a medium gray value and the class of background (the lung and the background) with a low gray value. In this study the range of possible numbers of clusters was set to $\{2, 3, \ldots, 7\}$ after which the optimal number of clusters (objects) by each validity functional was found.

TABLE I
FOUR VALIDATION FUNCTIONALS FOR FUZZY c-MEANS

Validity Index	Functional Description	Optimum Cluster nr.	Reference
Partition Coefficient	$V_{PC}(U) = \frac{1}{n}\left(\sum_{k=1}^{n}\sum_{i=1}^{c} u_{ik}^2\right)$	Max{ $V_{PC}(U, c_i, m)$ }	[29]
Partition Entropy	$V_{PE}(U) = -\frac{1}{n}\left(\sum_{k=1}^{n}\sum_{i=1}^{c} u_{ik} * \log_a(u_{ik})\right)$	Min{ $V_{PE}(U, c_i, m)$ }	[30]
Xie and Beni	$V_{XB}(U;V;X) = \frac{\sum_{i=1}^{c}\sum_{k=1}^{n} u_{ik}^{m} * \|x_k - v_i\|^2}{n * (\min\{v_i - v_j\})}$	Min{ $V_{XB}(U, c_i, m)$ }	[31]
Fukuyama & Sugeno	$V_{FSm}(U,V;X) = \sum_{i=1}^{c}\sum_{k=1}^{n} u_{ik}^{m}\left(\|x_k - v_i\|^2 - \|v_i - \bar{v}\|^2\right)$	Min{ $V_{FS}(U, c_i, m)$ }	[32]
Rezaee, et al.	$V_{CWB}(U,V) = Dis(c_{\max}) * Scat(c) + Dis(c)$ $Dis(c) = \frac{D_{\max}}{D_{\min}} * \sum_{k=1}^{c}\left(\sum_{z=1}^{c}\|v_k - v_z\|\right)^{-1}$ $Scat(c) = \frac{\frac{1}{c}\sum_{i=1}^{c}\|\sigma(v_i)\|}{\|\sigma(X)\|}$	Min{ $V_{CWB}(U, c_i, m)$}	[33]

Abbreviations: x_k is the k-th data point, v_i are cluster prototypes (cluster centers), c_i is the number of clusters, $\bar{v}$ is the grand mean of all data x_k and u_{ik} is the membership value of data x_k of class c_i. $\sigma(X)$ is the variance of the pattern set and $\sigma(v_i)$ is the fuzzy variance of the i-th cluster.

3) Parameters of the Study: All the images of the MR study were segmented twice by the two approaches described above. The split threshold factor α of (4) was equal to 0.1 and the decrease threshold factor β was set to 1.4. The average and the standard deviation of the gray values of each 3-D region in the bottom layer of the pyramid were used by FCM to segment images. The stop criterion value ε of FCM was set to 0.1; the iteration was stopped when the difference between two membership values at two successive iterations for all membership values was smaller than this threshold ε. The index V_{CWB} was used to find the number of clusters. The fuzzy index m had a fixed value of 2 and a Euclidean norm was used. For the application of the Hough transform the range of possible radii of LV lumen was set between 5 and 30 pixels.

III. IMAGE DATA

In this study, different sets of images were used. The synthetic and CT images were used as examples and segmentations of these images were judged visually. Segmentations of the MR images were validated quantitatively. In the following, the images will be described in more detail.

1) Synthetic Images: Two synthetic test images of size 128×128 that contain a disk object were created. These images were adopted from [35]. The object in these images had a constant intensity $(b + h)$ against a constant background intensity b. These images were convolved with a Gaussian kernel $(\sigma = 1.0)$; in addition, two realizations of white and colored noise were added so that different signal-noise ratios (SNR) were obtained. This ratio was defined as $10\log(h^2/\delta_N^2)$ dB, where δ_N was the standard deviation of the additive Gaussian noise.

2) CT Images: Two CT images were selected from spiral scans of the entire lung of a patient. These images were acquired with a Philips Tomoscan SR7000 (Philips Medical Systems, Best, The Netherlands), and were collected in our laboratory as part of an emphysema study; the current and voltage

were equal to 250 mA and 120 kVp, respectively. For the quantification measurement of clinical parameters the lungs had to be segmented out in those images.

3) MR Images: A set of 140 images was selected from multiphase, multislice short-axis Gradient Echo MR studies obtained from 10 abnormal subjects and 10 normal volunteers, men and women. For each abnormal subject a series of 6 images at mid-ventricle was selected from end-diastole to end-systole. For the normal subjects, the number of images was equal to 8. The images were acquired with a 0.5 Tesla (all normal subjects) and 1.5 Tesla (all abnormal subjects) MR system (Philips Medical Systems, Best, The Netherlands). The field of view was equal to 400×400 mm^2 and images had a size of 256×256 pixels and 12 bits of gray value resolution. Slice thickness and flip angle were equal to 10 mm and 50°, respectively. The echo time (TE) for normal subjects was equal to 9.4 ms and the Repetition Time (TR) was equal to the interval between two R peaks in the electrocardiogram. The TE for abnormal subjects was within a range of [12.7, 13.18] ms. The average age of the normal and abnormal subjects was 40.2 (range, 27–81 years) and 53.6 (range, 33–69 years), respectively. By applying bi-linear interpolation all images were enlarged with a zoom factor of four, after which the boundary of LV lumen (the endocardial contours with excluding papillary muscles) in each image was delineated manually by a specialist.

IV. Results

Examples: Fig. 3 shows some examples of the segmentation procedure applied to different images. The four images in each row represent from left to right the original image, the image segmented by the pyramidal segmentation, a fuzzy image of a specific class and the final segmentation after applying the MAX defuzzification method. The segmentation of two CT images of the lungs is shown in Fig. 3(a), while two examples of MRI images of the heart are shown in Fig. 3(b). The top and bottom rows represent the end diastolic and the end systolic image, respectively. The fuzzy images belong to the class of blood.

The segmentation of two synthetic images with a SNR of 10 dB are presented in Fig. 3(c). The left most images of the top and bottom rows were obtained by adding a colored and a white realization of Gaussian noise, respectively. For each image the fuzzy image of the class disk is also shown.

Results of MRI Evaluation Study:

A. Hough Transform

All images of each subject were analyzed by the Hough transform. The results of applying the Hough transform to all images of a subject were averaged to obtain an estimate of the center point of the LV lumen. In all cases, the estimated center point of LV lumens of all subjects was found to be within the LV lumens.

B. Processing Time

The total processing time for all 140 images was about 13 minutes on a Sun UltraSPARC 1 when the pyramidal segmentation in combination with FCM was applied. For this segmentation approach the majority of the processing time was needed for the Hough transform. The total processing time for all 140 images required by the first segmentation approach (applying only FCM) was about 34 minutes. This is an increase of roughly a factor of 3. The major processing time in the first approach was required by the fuzzy c-means and validity evaluations; for the evaluation of the new partitions (with a new number of clusters) the fuzzy c-means should run for a number of iterations, after which the membership values and the cluster centers (needed for the calculation of cluster validity indices) are defined.

C. Validity Indices

Table II shows the results of the five validity indices. In each row averages over 20 cases for a specific validation index are given. In the second column the optimal number of clusters found by the validity index averaged on MR images of 20 subjects is given. The third column gives the standard deviation of the number of clusters for all 20 subjects. Finally, the number of times that an index failed to find the true number $(c = 3)$ of clusters is shown on the last column (Number of errors). From Table II it is evident that the Fukuyama-Sugeno index V_{FS} and the partition entropy V_{PE} tend to overestimate the number of clusters. Although none of the indices found the optimum number of clusters in all VOI of the 20 subjects correctly, the validity index V_{CWB} found the optimal number of clusters in 15 VOI's.

D. Regression Study

A comparison between the manual definition of the amount of blood within the LV lumen and the two automated segmentation methods, 1) fuzzy c-means and 2) pyramidal segmentation combined with fuzzy c-means, is presented in Table III. Four regression studies were carried out to analyze the agreement. The parameters of each regression line are presented in a different column of Table III. The second column of this table shows the regression results for the manually and automatically defined LV in all 140 images of MR study, when only fuzzy c-means is applied. The third column shows the regression parameters for the end-diastolic (ED) images of 20 subjects using the same segmentation technique. As Table III illustrates, the segmentation method based on the pyramidal approach combined with fuzzy c-means has a higher regression coefficient and a lower offset than the segmentation based on fuzzy c-means alone.

The average amount of blood within the LV lumen of all 140 images, defined manually, was equal to 17.5 ml with a standard deviation (SD) of 6.9. For the 20 end-diastolic images the average was equal to 24.5 ml with a SD of 6.2. The differences between the automatically and the manually defined amount of blood are presented in Table IV. An average difference with a negative value indicates an underestimation. All differences reported in this table were statistically significant $(p < 0.05)$ except for one case. The difference between the manually defined LV lumen and the pyramidal segmentation combined with the fuzzy c-means was not statistically significant, and indicated a good agreement between the automatically and manually defined LV lumen. In contrast, the automatically detected LV lumen of four subjects in the end-diastolic images was overestimated by fuzzy c-means. The automatically labeled LV within a VOI included the right as well as the left ventricle.

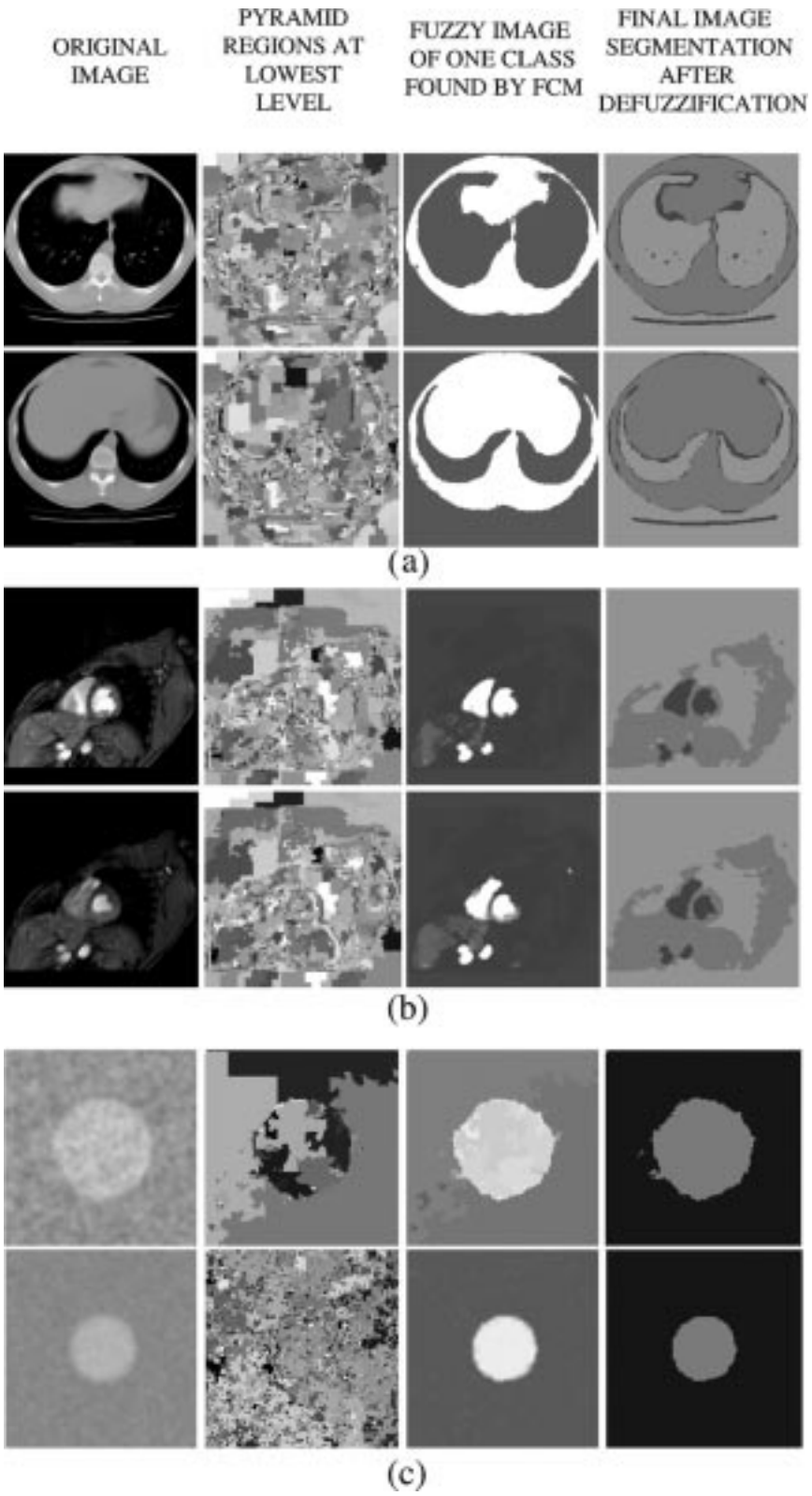

Fig. 3. Some examples of the segmentation procedure. From left to right: the original image, regions generated by the pyramidal segmentation, a fuzzy image and the segmentation result. (a) CT images of lung: the lung is included in the fuzzy class. The number of objects was set to 3. (b) MR images of the end-diastolic (top) and the end-systolic phase (bottom). The fuzzy class of blood is displayed. The number of objects was set to 3. (c) A synthetic image of a disk to which a correlated (top) and white noise (bottom) was added. The SNR value for both images is 10 dB.

V. Discussion

In this paper we have described an approach for the segmentation of a time-series of images. The combination of a pyramid data structure and fuzzy clustering was first proposed by Trivedi and Bezdek [15] who applied FCM as a region growing/merge algorithm to segment aerial images. In our approach however, the MR images are first split into a number of regions by a

TABLE II
AVERAGE OPTIMAL NUMBER OF CLUSTERS (ANATOMICAL OBJECTS WITHIN A VOLUME OF INTEREST) FOUND BY VALIDITY INDICES AVERAGED ON 20 MR IMAGE SERIES OF 20 SUBJECTS

Function	Mean of optimal c	Standard Deviation	Number of Errors (c=3 is correct)
V_{PC}	3.35	1.14	13
V_{PE}	6.75	0.44	20
			For all image series wrong optimal #
V_{XB}	3.55	1.54	14
V_{FS}	6.6	0.75	20
V_{CWB}	2.75	0.44	5

TABLE III
REGRESSION STUDY OF MEASUREMENT PAIRS OF THE AMOUNT OF BLOOD (IN MILLILITERS.) WITHIN THE LEFT VENTRICLE LUMEN DEFINED MANUALLY AND AUTOMATICALLY (BY TWO METHODS) FOR 140 IMAGES FROM TEN HEALTHY SUBJECTS AND TEN PATIENTS.

Abbreviations: FCM: Fuzzy C-Means; ED: end diastolic

Parameters	FCM		Pyramid and FCM	
	All images	ED images	All images	ED images
Offset [ml.]	7.58	11.23	6.49	2.24
R coefficient	0.86	0.79	0.90	0.94
X coefficient	0.76	0.57	0.92	0.99
Standard error of Coefficient	0.04	0.10	0.04	0.09

TABLE IV
DIFFERENCE BETWEEN THE AUTOMATICALLY AND THE MANUALLY MEASURED AMOUNTS OF BLOOD (IN MILLILITERS.) WITHIN THE LV LUMEN IN MR IMAGES OF 20 NORMAL AND PATIENT SUBJECTS DETERMINED BY TWO SEGMENTATION METHODS

Parameters	FCM		Pyramid and FCM	
	All images	ED images	All images	ED images
Mean	-3.0	2.43	-5.53	-2.09[α]
Standard deviation	6.4	9.87	3.03	2.15
Minimum	-11.7	-6.07	-13.08	-5.42
Maximum	27.5	27.50	1.10	1.10

Abbreviations: FCM: the fuzzy c-means; ED: end diastolic

[α] Not statistically significant (p = 0.15)

root labeling method and only the images at the bottom layer are merged by FCM. Despite [15] the issue of determining the number of regions c_i at the level i is studied in our method by means of a cluster validation procedure.

Our general segmentation procedure has a number of advantages. Firstly, it can be applied to any dimensional representation of an image series. Since some information required for a reliable segmentation is contained within the image series instead of a single image, it is more likely that by using this method, which preserves this information by its dimensional representation, a reliable segmentation will be achieved. Secondly, since objects through the various layers of the pyramid have their specific coarse representation, segmentation can be achieved at each resolution level of an image series. This may be preferred when, e.g., a specific object must be localized globally within the image series. The third advantage of our segmentation method is that the segmented images are fuzzy and therefore they can be used as the inputs of a reasoning system. Also, various defuzzification methods can be applied by which the performance of the segmentation for a specific application can be validated. A fourth advantage of this method is that the final segmentation can be achieved by a predefined number of objects. Since a general validation index for FCM has not been found yet, it is necessary to test a number of validation indices for a specific application, when the number of objects within the image is not known *a priori*. A reliable index might exist for a specific application, which can determine the number of objects automatically. Our results have shown that the V_{CWB} index proved to be the most reliable index among the five tested when applied to fuzzy partitions of segmentation data of MR images.

The results of the regression studies show that the amount of blood automatically defined by the pyramidal segmentation combined with FCM is more accurate than segmentation based on FCM only. Random errors represented in the standard deviation of the difference between the amount of the blood assessed manually and automatically was lower for the segmentation method based on pyramidal segmentation and FCM than the method based on FCM alone. The outliers of the regression study of the segmentation approach based on FCM alone mostly belong to the end-diastolic phase. The detected objects in this phase included the left as well as the right ventricle. This was reflected by a lower value of the regression coefficient $(r = 0.79)$ for the end-diastolic images compared with all images $(r = 0.86)$.

The automatically estimated amount of blood by both segmentation methods was lower than the amount defined manually. By visual inspection of the segmentation results we have found that in most images the automatically defined area of the LV lumen was systematically smaller than that defined by the expert. This phenomenon is also reported by Ranganath [7] and may be caused by a number of factors. The expert may draw the contour at the outside (beginning of the contrast change) pixels. In addition, the flow related artifacts in the LV lumen, motion artifacts and the partial volume effect will result in dark areas within the LV lumen. Therefore these effects will introduce a discrepancy between an automatic segmentation method, which looks for the white areas (blood within LV lumen), and the expert who is guided by an anatomical model in her/his mind and draws the lumen even where the contrast has vanished.

The expert has drawn contours within the images that were enlarged by a factor of 4 using bilinear interpolation, while the automatic segmentation is applied to the original images. This may also cause a systematic discrepancy.

The regression results of the pyramidal segmentation method combined with fuzzy c-means are in the same order as reported earlier. Our correlation coefficients were equal to 0.90 and 0.94 for all 140 images and 20 end-diastolic images, respectively. This coefficient reported by Zwehl *et al.* [36] using canine hearts and nearly ideal laboratory conditions was 0.92. Vandenberg *et al.* [37] reported a correlation coefficient of 0.92 using 119 observations of eight abnormal subjects. Although Chalana *et al.* [5] obtained a correlation coefficient of 0.95 for epicardial boundaries using initial contours, our segmentation method is a fully automatic approach.

Our MR study is directed to images of a slice between the apex and the base of the LV lumen. Although the validation study indicates a real opportunity for this segmentation technique, the reliability of this method must be further validated by an investigation based on more studies, especially using images near the apex or the base of the heart. The method must be validated for other imaging modalities as well.

In the pyramidal segmentation method we generated regions based on (dis)similarity measures (2) and (3). In other applications, these measures may be invalid, since they are based only on the statistics of the gray values. The evaluation of the parent-child relationship can be based on texture measurements, gradient information, etc., depending on the imaging modality and the characteristics of the object looked for. Since in general the small cardinality of the clusters, i.e. the number of feature vectors per cluster, can degrade the performance of segmentation, the effect of the parameters of the (dis)similarity measures, split threshold factor α of (4) and the decrease threshold factor β should be studied. In our studies, the values of these parameters, $\alpha = 0.1$ and $\beta = 1.4$, have been found empirically by trial and error. Although the noise contribution in our segmentation procedure is reduced by constructing a Gaussian (low-pass filter) pyramid, one may apply the possibilistic clustering approach [38] after applying FCM to eliminate noise feature vectors. In this case, the initial cluster centers should be provided by FCM.

The processing time of this segmentation approach may be reduced by replacing the FCM with a modified FCM suggested by Frigui and Krishnapuram [39] that finds the optimal number of clusters without repeating the clustering process and without the explicit use of a validity measure. This is the subject of our future studies.

ACKNOWLEDGMENT

The authors would like to thank the referees for their valuable comments and suggestions.

REFERENCES

[1] R. J. van der Geest, V. G. M. Buller, E. Jansen, H. J. Lamb, L. H. B. Baur, E. E. van der Wall, A. de Roos, and J. H. C. Reiber, "Comparison between manual and semiautomated analysis of left ventricular volume parameters from short-axis MR images," *J. Comput. Assist. Tomogr.*, vol. 21, no. 5, pp. 756–765, 1997.

[2] A. Boudraa, "Automated detection of the left ventricular region in magnetic resonance images by Fuzzy C-means model," *Int. J. Cardiac Imag.*, vol. 13, pp. 347–355, 1997.

[3] J. Weng, A. Singh, and M. Y. Chiu, "Learning-based ventricle detection from cardiac MR and CT images," *IEEE Trans. Med. Imag.*, vol. 16, no. 4, pp. 378–391, 1997.

[4] A. Yezzi, S. Kichenassamy, A. Kumar, P. Olver, and A. Tannenbaum, "A geometric snake model for segmentation of medical imagery," *IEEE. Trans. Med. Imag.*, vol. 16, no. 2, pp. 199–209, 1997.

[5] V. Chalana, D. T. Linker, D. R. Haynor, and Y. Kim, "A multiple active contour model for cardiac boundary detection on echocardiographic sequences," *IEEE Trans. Med. Imag.*, vol. 15, no. 3, pp. 290–298, 1996.

[6] D. L. Kraitchman, A. A. Yong, C. Chang, and L. Axel, "Semi-automatic tracking of myocardial motion in MR tagged images," *IEEE Trans. Med. Imag.*, vol. 14, no. 3, pp. 422–433, 1995.

[7] S. Ranganath, "Contour extraction from cardiac MRI studies using snakes," *IEEE Trans. Med. Imag.*, vol. 14, no. 2, pp. 328–338, 1995.

[8] D. R. Thedens, D. J. Skorton, and S. R. Fleagle, "Methods of graph searching for border detection in image sequences with application to cardiac magnetic resonance imaging," *IEEE Trans. Med. Imag.*, vol. 14, no. 1, pp. 42–55, 1995.

[9] A. Goshtasby and D. A. Turner, "Segmentation of cardiac cine MR images for extraction of right and left ventricular chambers," *IEEE Trans. Med. Imag.*, vol. 14, no. 1, pp. 56–64, 1995.

[10] M. R. Rezaee, C. Nyqvist, P. M. J. van der Zwet, E. Jansen, and J. H. C. Reiber, "Segmentation of MR images by a Fuzzy C-means algorithm," in *Proc. Computers Cardiology*, 1995, pp. 21–24.

[11] A. D. Parker, A. Hill, C. J. Taylor, T. F. Cootes, X. Y. Jin, and D. G. Gibson, "Application of point distribution models to the automated analysis of echocardiograms," in *Proc. Computers Cardiolgy*, 1994, pp. 25–28.

[12] J. G. Bosch, G. van Burken, S. S. Schukking, R. Wolff, A. J. van de Goor, and J. H. C. Reiber, "Real-time frame-to-frame automatic contour detection on echocardiograms," in *Proc. Computers Cardiology*, 1994, pp. 29–32.

[13] A. Boudraa, J. Mallet, J. Besson, S. Bouyoucef, and J. Champier, "Left ventricle automated detection method in gated isotopic ventriculography using fuzzy clustering," *IEEE Trans. Med. Imag.*, vol. 12, no. 3, pp. 451–465, 1993.

[14] M. D. Kelly, "Edge detection by computer using planning," *Mach. Intell.*, vol. 6, pp. 397–409, 1971.
[15] M. M. Trivedi and J. C. Bezdek, "Low level segmentation of aerial images with fuzzy clustering," *IEEE Trans. Syst., Man, Cybern.*, vol. SMC-16, no. 4, pp. 589–598, 1986.
[16] P. J. Burt, "The pyramid as a structure for efficient computation," in *Multiresolution Image Processing and Analysis*, A. Rosenfeld, Ed, Berlin, Germany: Springer-Verslag, 1984, pp. 6–35.
[17] J. R. Crowley, "A representation for shape based on peaks and ridges in the difference of low-pass transform," *IEEE Trans. Pattern Anal. Machine Intell.*, vol. PAMI-6, pp. 212–222, 1984.
[18] J. C. Bezdek, "Partition structures: A tutorial," in *The Analysis of Fuzzy Information*, J. C. Bezdek, Ed. Boca Raton, FL: CRC, 1987.
[19] L. O. Hall, A. M. Bensaid, L. Clarke, R. P. Velthuizen, M. Silbiger, and J. C. Bezdek, "A comparison of neural network and fuzzy clustering techniques in segmenting magnetic resonance images of the brain," *IEEE Trans. Neural Networks*, vol. 3–5, pp. 672–681, 1992.
[20] J. C. Bezdek, L. O. Hall, and L. P. Clarke, "Review of MR image segmentation techniques using pattern recognition," *Med. Phys.*, vol. 20, no. 4, pp. 1033–1048, 1993.
[21] M. C. Clark, L. O. Hall, D. B. Golgof, L. P. Clarke, R. P. Velthuizen, and M. S. Silbiger, "MRI segmentation using fuzzy clustering techniques," *IEEE Eng. Med. Biol. Mag.*, vol. 13, no. 5, pp. 730–742, 1994.
[22] A. M. Bensaid, L. O. Hall, J. C. Bezdek, L. P. Clarke, M. L. Silbiger, J. A. Arrington, and R. F. Murtagh, "Validity-guided (Re) clustering with application to image segmentation," *IEEE Trans. Fuzzy Syst.*, vol. 4, no. 2, pp. 112–123, 1996.
[23] D. P. Mukherjee, P. Pal, and J. Das, "Sodar image segmentation using fuzzy c-means," *Signal Process.*, vol. 54, no. 3, pp. 295–302, 1996.
[24] J. C. Bezdek, "Fuzzy Mathematics in Pattern Classification," Ph.D. dissertation, Appl. Math. Center, Cornell University, Ithaca, NY, 1973.
[25] J. C. Dunn, "A fuzzy relative of the ISODATA process and its use in detecting compact, well-separated cluster," *J. Cybern.*, vol. 3, pp. 32–57, 1974.
[26] R. N. Dave and K. Bhaswan, "Adaptive fuzzy c-shells clustering and detection of ellipses," *IEEE Trans. Neural Networks*, vol. 3, no. 5, pp. 643–662, 1992.
[27] R. Krishnapuram, O. Nasraoui, and H. Frigui, "The fuzzy C spherical shells algorithm: A new approach," *IEEE Trans. Neural Networks*, vol. 3-5, pp. 663–671, 1992.
[28] Y. Man and I. Gath, "Detection and separation of ring-shaped clusters using fuzzy clustering," *IEEE Trans. Pattern Anal. Machine Intell.*, vol. 16-8, pp. 855–861, 1994.
[29] J. C. Bezdek, "Cluster validity with fuzzy sets," *J. Cybern.*, vol. 3-3, pp. 58–72.
[30] ——, "Mathematical models for systematics and taxonomy," in *Proc. 8th Int Conf. Numerical Taxonomy*, G. Estabrook, Ed.. San Francisco, CA, 1975, pp. 134–166.
[31] X. L. Xie and G. A. Beni, "Validity measure for fuzzy clustering," *IEEE Trans. Pattern Anal. Machine Intell.*, vol. 13-8, pp. 841–846, 1991.
[32] Y. Fukuyama and M. Sugeno, "A new method of choosing the number of clusters for the fuzzy c-means method," in *Proc. 5th Fuzzy Systems Symp.*, 1989, pp. 247–250. in Japanese.
[33] M. R. Rezaee, B. P. F. Lelieveldt, and J. H. C. Reiber, "A new cluster validity index for the fuzzy c-means," *Pattern Recognit. Lett.*, vol. 19, pp. 237–246, 1998.
[34] H. K. Yuen, J. Princen, J. Illingworth, and J. Kittler, "Comparative study of hough transform methods for circle finding," *Image Vis. Comput.*, vol. 8-1, pp. 71–77, 1990.
[35] H. W. Meijering, "Segmentation of 3-D images using seeded volume growing," M.Sc. thesis, Elect. Eng., Delft Univ. Technol., Delft, The Netherlands, 1996.
[36] W. Zwehl, R. Levy, E. Garcia, R. Haendchen, W. Childs, S. Corday, S. Meerbaum, and E. Corday, "Validation of a computerized edge detection algorithm for quantitative two-dimensional echocardiography," *Circ.*, vol. 68, pp. 1127–1135, 1983.
[37] B. F. Vandenberg, L. S. Ruth, P. Stuhlmuller, H. E. Melton, and D. J. Skorton, "Estimation of left-ventricular cavity area with an on-line semi-automated echocardiographic edge detection system," *Circ.*, vol. 86, pp. 159–166, 1992.
[38] R. Krishnapuram and J. M. Keller, "A possibilistic approach to clustering," *IEEE Trans. Fuzzy Syst.*, vol. 1, no. 2, pp. 98–110, 1993.
[39] H. Frigui and R. Krishnapuram, "A robust algorithm for automatic extraction of an unknown number of clusters from noisy data," *Pattern Recognit. Lett.*, vol. 17, no. 12, pp. 1223–1232, 1996.

Mahmoud Ramze Rezaee received the M.Sc. degree from the Department of Electrical Engineering, Information Theory Group, Delft University of Technology, Delft, The Netherlands, in 1993. He received the Ph.D. degree from the Division of Image Processing, Leiden University Medical Center, Leiden, The Netherlands, in 1998.

His research interests are in the areas of fuzzy logic, (fuzzy) neural networks, pattern recognition, clustering, and medical image analysis. Since 1999, he has been with ALI Technologies, Vancouver, B.C., Canada.

Pieter M. J. van der Zwet received the M.Sc. degree from the Department of Electrical Engineering, Delft University of Technology, Delft, The Netherlands.

He was a Senior Research Associate with the Division of Image Processing from 1988 to 1997. His main interests are in the field of quantitative coronary angiography, knowledge-driven image segmentation, and blackboard systems for image analysis. He is currently with IBM Global Services, Amsterdam, The Netherlands.

Boudewijn P. F. Lelieveldt received the M.Sc. degree in 1994 from the Department of Mechanical Engineering, Delft University of Technology, Delft, The Netherlands, and the Ph.D. degree from the Division of Image Processing, Leiden University Medical Center (LUMC), Leiden, The Netherlands, in 1999.

He is currently a Senior Research Associate, coordinating the development of knowledge driven medical image segmentation methods at the Division of Image Processing, Department of Radiology, LUMC. His research interests are in the field of model based object recognition, knowledge-driven segmentation, and fuzzy logic.

Rob J. van der Geest received the M.Sc. degree from the Department of Electrical Engineering, Delft University of Technology, Delft, The Netherlands.

Since 1992, he has been a Senior Research Associate with the Division of Image Processing, Department of Radiology, Leiden University Medical Center, Leiden, The Netherlands, supervising the development of segmentation algorithms for the analysis of cardiovascular magnetic resonance images. His main expertise lies in the field of model-based segmentation and 3-D visualization.

Johan H. C. Reiber (S'73–M'75–SM'84) received the M.Sc. degree from the Delft University of Technology, Delft, The Netherlands, in 1971 and the Ph.D. degree in electrical engineering from Stanford University, Stanford, CA, in 1975.

He is a Professor of medical imaging with the Division of Image Processing, Department of Radiology, Leiden University Medical Center (LUMC), Leiden, The Netherlands, and the Inter-University Cardiology Institute of the Netherlands, Utrecht, The Netherlands. In 1977, he founded the Laboratory for Clinical and Experimental Image Processing (LKEB), Thoraxcenter, Rotterdam, The Netherlands, directing the research at the development and validation of objective and automated techniques for the segmentation of cardiovascular images, in particular for quantitative coronary arteriography (QCA), nuclear cardiology and echocardiography. With the move of LKEB in 1990 to LUMC, the scope broadened to intravascular ultrasound, MRI, CT, etc., also in radiological applications. His research interests include (knowledge guided) image processing and its clinical applications. Since 1990, he has been editor-in-chief of the *International Journal of Cardiac Imaging*.

Dr. Reiber is a Fellow of the European Society of Cardiology.